Optimal management of a microgrid Li-Ion battery considering non-linear losses using the Integer Zig-Zag formulation

Javier García-González
Salvador Guerrero
Institute for Research in Technology (IIT),
ICAI School of Engineering, Pontifical Comillas University
Madrid, Spain
javiergg@comillas.edu, salvadorgg@alu.comillas.edu

***Abstract*—This paper presents a model for optimizing the management of a Li-Ion battery in a microgrid, considering the presence of nonlinear losses during the charging and discharging processes. The paper examines the nature of these losses and proposes updated nonlinear expressions that depend on the state of charge and on the charging or discharging power. The piecewise linear approximations of the losses bivariate functions are implemented using the novel integer zig-zag (ZZI) formulation. The corresponding ZZI constraints are integrated into an optimization model to determine the optimal schedule for a residential isolated microgrid comprising a solar panel, a diesel generator, and a Li-Ion battery. The case study compares different triangulation strategies regarding their impact on the quality of the obtained solution and the computational burden.**

***Index Terms*—Energy management system, microgrid, non-linear losses, steady-state, zig-zag.**

NOMENCLATURE

For the sake of simplicity, this nomenclature omits all terms specific to the ZZI formulation, which will be elaborated upon in section III.

A. Sets

$t \in \mathcal{T}$	time periods {1 to T}

B. Parameters

D_t	Demand at each time period t, [kW]
Δ_t	Duration of each time period t, [h]
a, b, c	Quadratic, linear, and constant terms of the diesel cost function, [€/h/(kW)^2], [€/kWh], [€/h]
E_o	Initial energy stored at the battery, [kWh]
$\overline{P}^d$	Maximum capacity of the diesel generator, [kWh]
$\overline{P}^{disc}$	Maximum discharge power of the battery, [kW]
$\overline{P}^{cha}$	Maximum charge power of the battery, [kW]
$\overline{E}$, $\underline{E}$	Maximum and minimum stored energy [kWh]

C. Variables

e_t	Energy stored at the end t [kWh]
p_t^{char}	Power consumed by the battery in t [kW]
p_t^{disc}	Power generated by the battery in t [kW]
$p_{loss,t}^{cha}$	Power losses when charging in t [kW]
$p_{loss,t}^{disc}$	Power losses when discharging in t [kW]
p_t^{pv}	Power produced by the PV panel in t [kW]
p_t^{pns}	Non-served power in period t [kW]
u_t^d	Commitment of the diesel generator in t {0,1}
u_t^{disc}	Battery discharge decision in t {0,1}
u_t^{cha}	Battery charge decision in t {0,1}

I. INTRODUCTION

Li-Ion batteries are expected to play a crucial role in the decarbonization of the electric power industry due to their ability to store electricity efficiently and provide a reliable and flexible power source. The optimal operation of a battery can be obtained by solving a mathematical programming problem considering as decision variables the power that can be charged or discharged and the level of energy stored at any given moment. In this sense, from the optimization point of view, one of the challenges is the presence of non-linear losses during both the charging and discharging processes. This paper presents a battery optimization model considering non-linear losses. This is achieved by means of the general integer zig-zag (ZZI) formulation proposed in [1] that provides an efficient non-convex piecewise linear approximation of univariate and bivariate functions. In particular, the loss functions are expressed in terms of the State of Charge (SoC) and the power charged/discharged, and this approach improves the accuracy of the results while significantly reducing the computational burden compared to other mixed-integer linear programming techniques. To illustrate the application of this method, an optimization model of a microgrid has been implemented as in these installations, the optimal battery management is essential for achieving an efficient operation [2]. The main contributions of this paper are the following: First, the paper provides updated non-linear expressions to approximate the

Submitted to the 23rd Power Systems Computation Conference (PSCC 2024).

charging and discharging losses of Li-ion batteries that can be used in steady-state analyses for the energy management of a microgrid. Second, the novel ZZI technique is proposed to approximate those losses by accurate and efficient piecewise linear approximations that can be embedded in optimization-based models. Finally, a comparison of different triangulation strategies is provided.

The paper is organized as follows: Section II proposes the nonlinear expressions for the loss functions. Section III explains the ZZI method. Section IV presents the optimization model of a microgrid considering the mentioned nonlinear losses. In Section V, the case study is presented, and finally, Section VI summarizes the most relevant conclusions.

II. Expressions of Battery Losses

A. Non-linear behavior of the battery

Batteries are highly complex systems, and their modeling should balance accuracy and computational efficiency. In [3], a review is presented on the various alternatives available in the literature to model Li-Ion batteries. [4] is a classical paper that presents an equation that describes the discharge behavior of a battery that is deduced by analyzing the cathode and anode potential during the discharge process, assuming that both electrodes have porous active materials, that the electrolyte resistance is constant, that the cell is discharged at a constant current, and that the polarization is a linear function of the active material current density:

$$V_{batt} = E_o - R \cdot i - K\frac{Q}{Q - it}i + A \cdot e^{-B \cdot \frac{it}{Q}} \quad (1)$$

where V_{batt} (V) is a time-dependent variable that expresses the voltage between the terminals of the battery, E_o (V) is the constant potential of the cell (sum of the corresponding terms for the anode and cathode) that could be interpreted as the open-circuit battery voltage if the exponential term were disregarded, R (Ω) is the internal resistance, i (A) is the current withdrawn from the battery, K (Ω) is the polarization coefficient, Q (A·h) is the amount of available charge, it (A·h) is the amount of charge that has been obtained from the battery at time t measured since the moment that the discharge started, and A (V) and B (dimensionless) are empirical constants to model the initial exponential drop expressed in the last term of (1). In posterior papers, the exponential term is expressed as $A \cdot e^{-B \cdot it}$, and therefore the units of B are $(\text{A·h})^{-1}$. The empirical values of E_o, K, Q, R, A, and B can be determined by fitting the equation numerically to discharge data obtained through experiments.

In [5], the authors take as a starting point a similar equation as (1), but introduce some improvements to consider the varying nature of the current: $it = \int_0^t i \cdot dt$.

In this case, the obtained expression for the Li-Ion battery discharge process is the following one, where the current satisfies that $i > 0$:

$$V_{batt}^{disc} = E_o - R \cdot i - K\frac{Q_m}{Q_m - it}(it + i^*) + A \cdot e^{-B \cdot it} \quad (2)$$

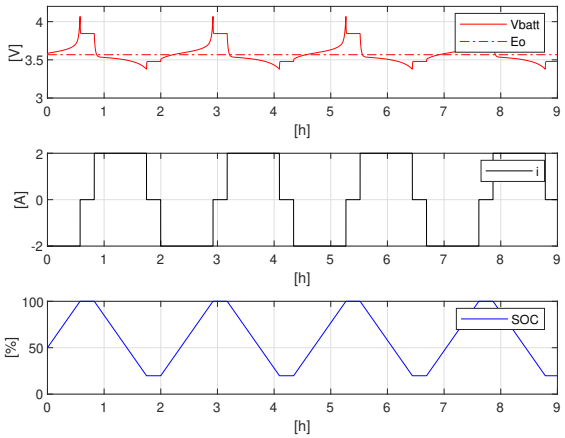

Fig. 1. Simulated example of charge and discharge cycles of a Li-Ion battery.

where the term i^* (A) is the low-pass filtered current flowing through the polarisation resistance that helps to carry out the numerical simulations with a typical value of the time constant equal to $\tau = 10$ s, Q_m (A·h) represents now the maximum battery capacity, and the coefficient B ($(\text{A·h})^{-1}$) has been adapted from (1) taking into account the value Q_m.

In addition, based on [5], the resulting expression for the charging process is the following one where the current satisfies that $i < 0$:

$$V_{batt}^{char} = E_o - R \cdot i - K\frac{Q_m}{Q_m - it}it - K\frac{Q_m}{it + 0.1 \cdot Q_m}i^* + A \cdot e^{-B \cdot it} \quad (3)$$

Notice that in (3), the polarisation resistance is shifted by about 10% of the capacity of the battery to reflect experimental results when the battery is fully charged ($it = 0$).

Let us define the polarization resistance R_{pol} as follows:

$$R_{pol}(i) = \begin{cases} K\frac{Q_m}{Q_m - it} & \text{if } i > 0 \\ K\frac{Q_m}{it + 0.1 \cdot Q_m} & \text{if } i \leq 0 \end{cases} \quad (4)$$

Then, the general expression for V_{bat} valid for both the charging and discharging processes is the following one:

$$V_{batt} = E_o - R \cdot i - R_{pol}i^* - K\frac{Q_m}{Q_m - it}it + A \cdot e^{-B \cdot it} \quad (5)$$

These expressions have been tested with the battery model from the Simscape Electrical™, Specialized Power Systems Library, [6]. The voltage of the battery under controlled current (-2, 0, +2 A) is shown in the first subplot of Figure 1, along with the resulting (SoC) starting at 50%. In this example, a minimum discharge value of 20% was set to stop the discharge process, with a delay of 15 minutes between both the charging and discharging processes where the current is null.

Instead of modeling the polarization resistance in terms of it, working directly with the SoC may be more convenient. Let us define the SoC as the ratio between the stored charges in a particular moment and the maximum capacity. Assuming that

initially the battery is fully charged, the following expression can be applied:

$$SOC = \frac{Q_m - \int_0^t i \cdot dt}{Q_m} = \frac{Q_m - it}{Q_m} \tag{6}$$

yielding to:

$$it = Q_m(1 - SOC) \tag{7}$$

B. Losses in terms of the current

When current flows through the battery's internal resistance, some electrical energy is converted into heat due to the Joule effect. This heat leads to a loss of energy in the battery and can cause the battery to heat up. In addition, during charging and discharging, a series of complex electrochemical reactions occur in the battery's electrodes and the electrolyte. As these reactions are not 100% efficient, a small amount of energy is lost as heat. To illustrate this phenomenon, one can assess the product of the battery current and each of the four terms constituting the voltage drop across the battery obtained from (5):

$$\begin{aligned}(E_o - V_{batt})i = &\underbrace{R \cdot i^2}_{\text{Term1}} + \underbrace{R_{pol} \cdot i^* \cdot i}_{\text{Term2}} \\ &+ \underbrace{(\frac{Q_m}{Q_m - it} it)i}_{\text{Term3}} - \underbrace{(A \cdot e^{-B \cdot it})i}_{\text{Term4}}\end{aligned} \tag{8}$$

In Figure 2, the temporal evolution of each of the four terms is displayed. The first term represents the Joule losses within the battery's internal resistance. The battery begins with an initial state of charge (SOC) of 50% and charges until it reaches its maximum capacity. Subsequently, there is a 15-minute waiting period, followed by discharge until the SOC reaches 20%. After another 15-minute wait, this pattern repeats consistently. During both the charging and discharging processes, the power associated with the first term remains consistently positive, signifying losses as expected within a resistance with a constant value. This results in a square wave in the dissipated power. A similar phenomenon occurs with the second term; however, in this case, since the polarization resistance depends on the SOC, the instantaneous losses also vary over time while remaining consistently positive. Conversely, the third and fourth terms exhibit a pattern alternating between positive and negative power.

This paper proposes not to include terms 3 and 4 in the loss function, and therefore, the proposed expression of the instantaneous battery losses is the one shown in (9):

$$p_{loss} \approx \underbrace{R \cdot i^2}_{\text{Term1}} + \underbrace{R_{pol} \cdot i^* \cdot i}_{\text{Term2}} \tag{9}$$

The time intervals for collecting and analyzing time series data can vary depending on the application and system requirements. In a stationary battery system, the Energy Management System (EMS) can use periods of several minutes to monitor the state of charge and discharge, as well as other factors

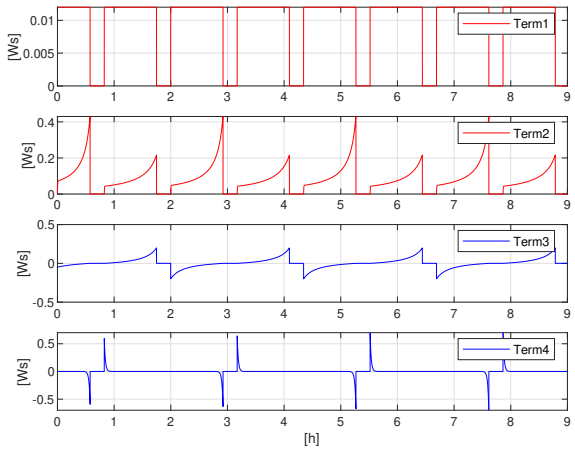

Fig. 2. Simulated example of charge and discharge cycles of a Li-Ion battery.

such as temperature and ambient conditions. Thus, for the EMS problem in which transient effects are disregarded and a steady-state approach is employed, the filtered current can be assumed to be equivalent to the average steady-state current in the considered discrete time period. Denoting as I [A] the average current in such interval of time, then the corresponding average losses can be expressed as follows:

$$p_{loss} = (R + R_{pol}) \cdot I^2 \tag{10}$$

Taking into account the expressions in (4) and (7), the expressions of the losses [kW] proposed in this paper for the battery discharge and charge losses are the following ones:

$$p_{loss,t}^{disc} = 10^{-3}(R + \frac{K}{soc_t})I^2 \tag{11}$$

$$P_{loss}^{char} = 10^{-3}(R + \frac{K}{1.1 - soc_t})I^2 \tag{12}$$

C. Losses in terms of the power

Assuming that the battery power is expressed in [kW], and denoted by V_r (V) the rated battery voltage, the current can be approximated as follows:

$$I \approx \begin{cases} +10^3 \frac{P^{disc}}{V_r} & \text{if } discharge \\ -10^3 \frac{P^{char}}{V_r} & \text{if } charge \end{cases} \tag{13}$$

This allows us to express the losses of the battery as shown in the expressions (14) and (15), which have a quadratic behavior for the power and hyperbolic for the SoC:

$$p_{loss,t}^{disc} = 10^3(R + \frac{K}{soc_t})(\frac{p_t^{disc}}{V_r})^2 \tag{14}$$

$$p_{loss,t}^{char} = 10^3(R + \frac{K}{1.1 - soc_t})(\frac{p_t^{char}}{V_r})^2 \tag{15}$$

Notice that expressions (14) and (15) differ from the expressions presented in [7] in equations (13) and (14). The reasons for such discrepancies are twofold. First, the empirical 10%

correction explained previously in (3) leads to a denominator in one of the terms of the charging case equal to $0.9 - soc$ instead of $1.1 - soc$. This issue is later corrected in [8] that uses the proposed denominator $1.1 - soc$ that is also coherent with the expressions used in the battery library available in [6]. Second, when the authors of [7] obtain the expressions in terms of power instead of current, they consider Term 3 in (8) as losses. This issue is also inherited in paper [8], see equations (1) and (2). Consequently, the losses estimated in the numerical simulations carried out in those papers might be overestimated.

In any case, although this paper uses the expressions of the losses (14) and (15), the method proposed here is entirely general and would allow approximating any nonlinear loss function as long as it exhibits a dependency on two variables (power and SoC in this case), as the Zig-Zag method is limited to univariate or bivariate functions.

III. Integer Zig-Zag formulation

The approximation of non-linear and non-convex functions by piecewise linear functions is common in operations research applied to real-world problems. A popular approach was first presented in [9], and according to [10], it is the most common method available in the literature. The basic idea is to split the entire domain of two independent variables into non-overlapping triangles. Then, auxiliary binary variables are used to ensure that only one triangle is active at a time. This formulation, referred to as C-K1, has been included in the appendix and will be used as a benchmark in the study case.

In recent years, more efficient formulations have been proposed. For instance, [11] introduces a formulation for piecewise linear functions of one and two variables that use a number of binary variables and extra constraints logarithmic in the number of linear pieces of the functions, and they prove that the new formulations have favorable tightness properties that result in better computational performance than other mixed integer binary formulations. Later on, the binary and integer zig-zag formulations (ZZB and ZZI, respectively) were proposed in [1], providing an efficient non-convex piecewise linear approximation of univariate and bivariate functions.

According to the numerical results of [1] and [12], where this technique is applied successfully to model net-head hydro units, ZZI outperforms ZZB. For that reason, this method is summarized hereafter to understand its applicability for modeling the non-linear losses of the battery.

A. ZZI mathematical formulation

Let $z = f(x, y)$ be a continuous non-linear bivariate function (it can be non-convex), defined over the domain $[\underline{x}, \overline{x}] \times [\underline{y}, \overline{y}]$. The function $f(x, y)$ can be piecewise linearized by performing a triangulation of the domain over which the function is defined and imposing that for points lying in between any given triangle, the function is approximated by the linear combination of its three vertices. The first step is to build the triangular mesh. This can be achieved by creating a rectangular grid where the x and y domains are discretized in $n+1$ and $m+1$ values: $\hat{x}_i, \forall i \in I = \{1, \cdots, n+1\}$ and $\hat{y}_j, \forall j \in J = \{1, \cdots, m+1\}$. Thus, the x-axis is split into n intervals, and the y-axis is split into m intervals. Then, it is necessary to define the triangles. Given a rectangle, it is possible to define four possible triangles resulting from connecting the opposed vertices by a diagonal (southwest to northeast) or by an anti-diagonal (southeast to northwest). For instance, anti-diagonal connections have been used in Figure 3, while both diagonal and anti-diagonal connections appear in the Union-Jack triangulation shown in Figure 4.

In order to compute the linear combination of the triangle vertices, let's define the continuous variables $\theta_{i,j} \in [0, 1]$ as the weights used to compute the convex combination. Assuming that only tree adjacent vertices can have a value of $\theta_{i,j}$ different from zero (which will be ensured later on by a set of additional constraints), the convex combination can be obtained as shown in (16):

$$x = \sum_{i \in I} \sum_{j \in J} \theta_{ij} \cdot \hat{x}_i \tag{16a}$$

$$y = \sum_{i \in I} \sum_{j \in J} \theta_{ij} \cdot \hat{y}_j \tag{16b}$$

$$z = \sum_{i \in I} \sum_{j \in J} \theta_{ij} \cdot f(\hat{x}_i, \hat{y}_j) \tag{16c}$$

$$\sum_{i \in I} \sum_{j \in J} \theta_{ij} = 1 \tag{16d}$$

$$0 \leq \theta_{ij} \leq 1 \quad \forall i \in I, \forall j \in J \tag{16e}$$

Let's denote *column* a particular index $i \in I$ and *row* a particular index $j \in J$. The intuitive idea of this method is to ensure that the values of $\theta_{i,j}$ can only assume non-zero values for two adjacent columns and two adjacent rows. This is known as a special ordered set of type 2 (SOS2) constraints, and among the SOS2 formulations available in the literature, the zig-zag method is very efficient from the computational perspective. The application of the zig-zag method to uni-variate functions requires to build previously the integer encoding matrix $\mathbf{C}^\nu$ with dimension $(d \times \nu)$ where ν is a positive integer and $d = 2^\nu$. The recursive expression (17) presented in ([1]) can be used to build this matrix for any value of ν, taking into account that C_d^ν is a row vector obtained by extracting the d-th row from matrix $\mathbf{C}^\nu$, $\mathbf{C}^1 = (0, 1)^T$, and $\mathbf{0}^d$ and $\mathbf{1}^d$ are column vectors with dimension d filled with zeros and ones respectively.

$$\mathbf{C}^{\nu+1} = \begin{pmatrix} \mathbf{C}^\nu & \mathbf{0}^d \\ \mathbf{C}^\nu + \mathbf{1}^d \cdot C_d^\nu & \mathbf{1}^d \end{pmatrix} \tag{17}$$

The expression (17) can be used to build the two matrices needed for the bivariate functions: $\mathbf{C}^s$ to formulate the SOS2 constraints that ensure that only two adjacent columns are active and $\mathbf{C}^r$ to formulate the SOS2 constraints that ensure that only two adjacent rows are active. The values of s and r depend on the size of the selected grid and can be computed as

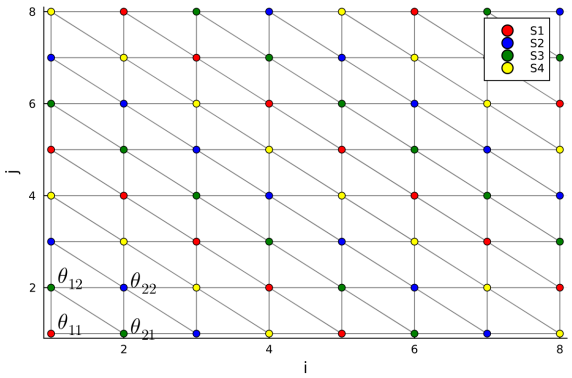

Fig. 3. 8×8 grid with the K1 triangulation pattern.

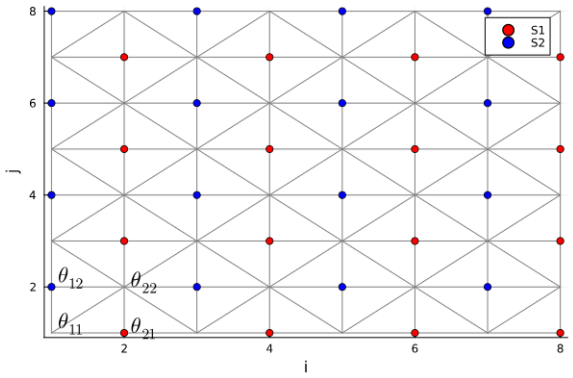

Fig. 4. 8×8 grid with the J1 triangulation pattern.

follows using the ceil function ($\lceil a \rceil$:= smallest integer greater or equal than a): $s = \lceil log_2(n) \rceil$, and $r = \lceil log_2(m) \rceil$

Once the four vertices of the rectangle defined by the two active columns and the two active rows of the grid have been selected, the next step is to select a triangle among the ones that can be formed in that rectangle. Therefore, the whole triangle selection process can be broken down into three groups of constraints: 1) *adjacent columns selection*, 2) *adjacent rows selection*, and 3) *triangle selection*.

1) Adjacent columns selection: It is necessary to define the integer variable $\zeta_g^{col} \in \mathbb{Z}$ where g is an auxiliary integer index and to apply the constraints shown in (18) $\forall g \in [1, s]_{\mathbb{Z}}$:

$$\sum_{i \in I} C_{i-1,g}^{s} \left(\sum_{j \in J} \theta_{ij} \right) \leq \zeta_g^{col} \leq \sum_{i \in I} C_{i,g}^{s} \left(\sum_{j \in J} \theta_{ij} \right) \quad (18a)$$

$$0 \leq \zeta_g^{col} \leq 2^{s-g} \quad (18b)$$

Notice that in (18) $C_{i,j}^{s}$ represents the element (i, j) of the matrix, and it has been assumed that $C_0^s \equiv C_1^s$, and $C_{n+1}^s \equiv C_n^s$ for notation simplicity.

2) Adjacent rows selection: Analogously, it is necessary to define the integer variable $\zeta_k^{row} \in \mathbb{Z}$ where k is an auxiliary integer index and to apply the constraints shown in (19) $\forall k \in [1, r]_{\mathbb{Z}}$. In this case, it is also assumed that $C_0^r \equiv C_1^r$, and $C_{m+1}^r \equiv C_m^r$.

$$\sum_{j \in J} C_{j-1,k}^{r} \left(\sum_{i \in I} \theta_{ij} \right) \leq \zeta_k^{row} \leq \sum_{j \in J} C_{j,k}^{r} \left(\sum_{i \in I} \theta_{ij} \right) \quad (19a)$$

$$0 \leq \zeta_k^{row} \leq 2^{r-k} \quad (19b)$$

3) Triangle selection: Once the four vertices of the active rectangle have been selected, the selection of one unique triangle can be achieved by different methods. In case the K1 triangulation is chosen, then equations (20) and (21) must be considered, where it is necessary to define the binary variables z_1 and z_2. In the case of choosing the union-jack triangulation, only one binary variable is required, and the required constraints are the ones shown in (22) and (23).

$$\begin{aligned} \sum_{(i,j) \in S_1} \theta_{i,j} \leq z_1 \qquad & \sum_{(i,j) \in S_2} \theta_{i,j} \leq 1 - z_1 \\ \sum_{(i,j) \in S_3} \theta_{i,j} \leq z_2 \qquad & \sum_{(i,j) \in S_4} \theta_{i,j} \leq 1 - z_2 \end{aligned} \quad (20)$$

$$z_1, z_2 \in \{0, 1\}$$

$$\begin{aligned} S1 &= \{(i,j) : i + j \equiv 2 \mod 4\} \\ S2 &= \{(i,j) : i + j \equiv 0 \mod 4\} \\ S3 &= \{(i,j) : i + j \equiv 1 \mod 4\} \\ S4 &= \{(i,j) : i + j \equiv 3 \mod 4\} \end{aligned} \quad (21)$$

$$\sum_{(i,j) \in S_1} \theta_{ij} \leq z_1 \qquad \sum_{(i,j) \in S_2} \theta_{ij} \leq 1 - z_1 \quad (22)$$

$$z_1 \in \{0, 1\}$$

$$\begin{aligned} S1 &= \{(i,j) : i \text{ is even and } j \text{ is odd}\} \\ S2 &= \{(i,j) : j \text{ is even and } i \text{ is odd}\} \end{aligned} \quad (23)$$

IV. Model

A. Objective function

The objective function (24) is to minimize the sum for all the periods of the diesel generation cost plus the possible non-served energy cost:

$$\min \sum_{t} [a \cdot (p_t^d)^2 + b \cdot p_t^d + c \cdot u_t^d + c_{pns} \cdot p_t^{pns}] \cdot \Delta_t \quad (24)$$

Notice that in (24), the commitment status of the diesel generator multiplies the independent term of the cost function, as such cost is only incurred when the diesel generator is functioning.

B. Constraints

The demand balance equation (25) establishes that the demand D_t has to be satisfied by the PV generation p_t^{pv}, plus the diesel generation p_t^d, plus the power injected by the battery during the discharge p_t^{disc}, minus the power consumed during the battery during the charging process p_t^{char}. In the event that

there is not enough generation to meet the demand, the slack variable p_t^{pns}would be activated:

$$p_t^{pv} + p_t^d + p_t^{disc} - p_t^{char} + p_t^{pns} = D_t, \forall t \in T \tag{25}$$

In numerous EMS applications, rather than employing voltage or current as control variables, the focus is placed on the power generated or consumed by the battery. For this reason, only quantities related to the power and energy of the battery will be used in this formulation. In a battery, the SoC measures the percentage of electrical charge stored at a given moment in relation to the maximum charge it could hold, considering the battery's nominal capacity. Since voltages or currents in the battery are not modeled, it is proposed to approximate the SoC using energy-related quantities rather than charge-related ones. The energy balance equation (26) expresses the energy content in the battery at the end of each period e_t taking into account the charging and discharging processes where e_{t-1} for $t = 1$ is equal to the initial charge of the battery E_o:

$$e_t = e_{t-1} + [(p_t^{char} - p_{loss,t}^{char}) - (p_t^{disc} + p_{loss,t}^{disc})]\Delta_t, \forall t \in T \tag{26}$$

As e_t is an instantaneous value at the end of each discrete time period, this paper proposes to approximate the SoC at each time step in terms of the average value of the energy content at the beginning and at the end of each period:

$$soc_t = \frac{\frac{1}{2}(e_{t-1} + e_t)}{\overline{E}} \tag{27}$$

Regarding the battery losses, the expressions (14) and (15) are considered and the ZZI method explained in section III is replicated for all the variables $p_{loss,t}^{char}$ and $p_{loss,t}^{disc}$.

The unit-commitment constraint of the diesel generator (28) ensures that it cannot produce when it is off:

$$p_t^d \leq u_t^d \cdot \overline{P}^d, \forall t \in T \tag{28}$$

To prevent the battery from charging and discharging at the same time, the equations (29a) and (29b) are taken into account, and (29c) imposes that only a mode of operation is possible during the same hour:

$$p_t^{char} \leq u_t^{cha} \cdot \overline{P}^{cha}, \forall t \in T \tag{29a}$$
$$p_t^{disc} \leq u_t^{disc} \cdot \overline{P}^{cha}, \forall t \in T \tag{29b}$$
$$u_t^{disc} + u_t^{char} \leq 1, \forall t \in T \tag{29c}$$

Finally, the bounds of the decision variables are the following ones:

$$\underline{E} \leq e_t \leq \overline{E}, \forall t \in T \tag{30a}$$
$$0 \leq p_t^{pv} \leq P_t^{pv}, \forall t \in T \tag{30b}$$
$$0 \leq p_t^{disc} \leq \overline{P}^{disc}, \forall t \in T \tag{30c}$$
$$0 \leq p_t^{char} \leq \overline{P}^{cha}, \forall t \in T \tag{30d}$$
$$0 \leq p_t^{pns}, \forall t \in T \tag{30e}$$

TABLE I
MICROGRID PARAMETERS

Load	$D_{\max}$	1.47	[kW]
Solar Panel	$P_{\max}^{pv}$	2	[kW]
Diesel	$P_{\max}^{d}$	1.0	[kW]
	c	0.0157	[€]
	b	0.1080	[€/kW]
	a	0.3100	[€/kW^2]
Li-Ion battery	$\overline{E}$	2.9	[kWh]
	$\overline{E_0}$	0	[kWh]
	$\overline{P}^{cha}$	2.9	[kW]
	$\overline{P}^{disc}$	2.9	[kW]
	K	8.0625	[mΩ]
	R	26.46	[mΩ]
	V_r	51.2	[V]
	c_{ens}	1	[€/kWh]

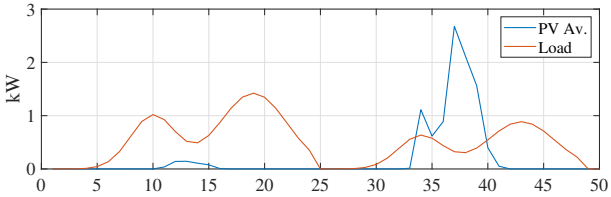

Fig. 5. Hourly load and available PV

V. STUDY CASE

This section presents the results obtained with a microgrid taken from [13], which comprises a PV panel, a Li-Ion battery, and a diesel generator (see Table I). The analysis has been carried out for various grid sizes, for the two explored zig-zag triangulations (ZZI-K1 and ZZI-J1) and for the classic formulation C-K1. A relative tolerance of 0.5% has been chosen as the termination criterion for the resulting mixed-integer quadratic programming (MIQP) problems solved by commercial solvers CPLEX 22.1.1.0 and GUROBI 10.0.3. First, the results for a 48-hour horizon are presented, and subsequently, the analysis is extended for two 168-hour cases.

A. Optimal management for a 48-hour scope

Figure 5 shows the hourly and the available PV profiles over a 48-hour period. These two consecutive days were selected to explore a scenario encompassing extreme conditions: a heavily overcast day with minimal PV generation and a clear, sunny day. Figure 6 shows the results obtained with ZZI-J1 using a 8×8 grid. On the first day, both the generator and the battery are required to meet the demand during the peak demand hours. On the other hand, since the peak solar irradiation hours do not align with the demand peaks on the second day, this solar production is utilized to charge the battery. Subsequently, this stored energy is used to meet the load requirements. Additionally, it can be seen that the hourly average SoC throughout the entire horizon respects the 10% and 100% limits.

B. Optimal management for two 168-hour scopes

In order to assess the performance of both zig-zag formulations in the case of a larger-scale problem, the models have

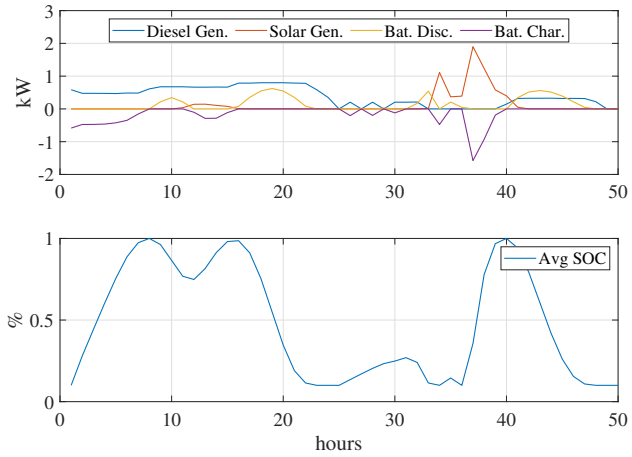

Fig. 6. Obtained results (ZZI-J1 8×8, GUROBI)

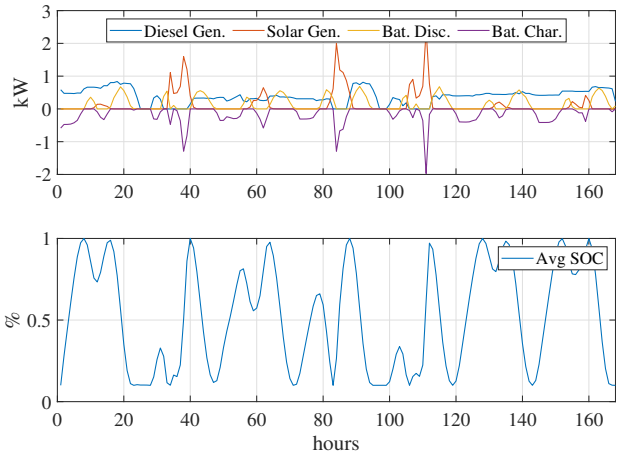

Fig. 8. Obtained results (ZZI-J1 8×8, GUROBI, Winter)

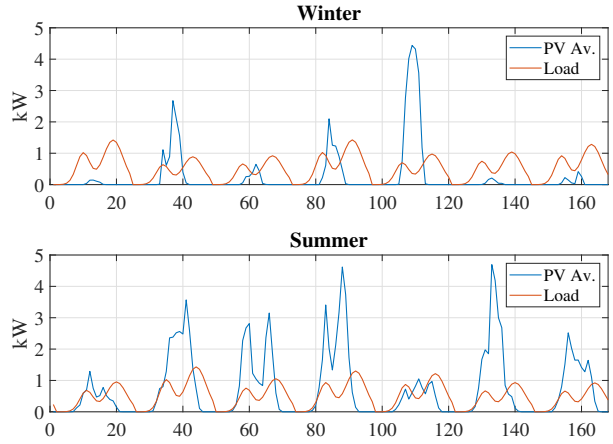

Fig. 7. Hourly load and available PV

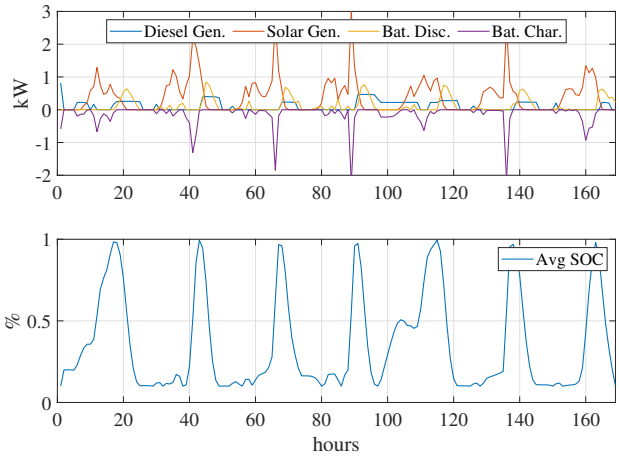

Fig. 9. Obtained results (ZZI-J1 8×8, GUROBI, Summer)

been run for one week in summer (168h_S) and one week in winter (168h_W). Figure 7 depicts both weeks' demand and available solar production time series. The obtained results are presented in Figures 8 and 9. In winter, the diesel generator plays a much more prominent role, and the battery management becomes more demanding to leverage solar production during the limited available hours while ensuring sufficient energy reserves to satisfy the demand. However, in summer, it is observed that the battery is mainly managed to harness the surplus during peak solar production hours when demand is already met.

C. *Computational performance*

Table II compares the model's performance for different configurations. GUROBI outperforms CPLEX with an average execution time between 30 and 115 times faster in the 48h scenarios where both solvers provided solutions. Empty cells indicate that the solver has been unable to find an integer solution within the 1-hour time limit. Except for small cases with the lowest grid resolution, the results indicate that methods based on the zig-zag formulation are significantly superior to the classical formulation: 12.1 faster on average for the analyzed cases where all the methods provided a solution for the 8×8 grid. In the case of the weekly execution with a high level of detail, the ZZI-J1 formulation stands out compared to other methods as it allows for finding a solution. This suggests that for large-scale problems with a high level of grid granularity, the ZZI-J1 method should be preferred.

APPENDIX: CLASSIC FORMULATION (C-K1)

This appendix includes the formulation of the classical piecewise linear approximation method for functions of two variables presented in [9]. The original expressions have been adapted to align with the nomenclature used in this paper and the K1 triangulation, aiming to simplify the comparison. Therefore, for a point (i, j) of the mesh, its upper (^{u}) and lower (^{l}) adjacent triangles can be defined as illustrated in Figure 10. For each upper triangle, it is necessary to define a binary variable called $\zeta^u_{i,j} \in \{0, 1\}\ \forall i \in I\ , \forall j \in J$. Similarly, binary variables $\zeta^l_{i,j} \in \{0, 1\}$ are defined for each lower triangle. The

TABLE II
SUMMARY OF COMPUTATIONAL PERFORMANCE.

Case	Grid	Method.	Solver	Obj.[€]	Time [s]	Rel.Gap
48h	4x4	ZZI-J1	cplex	6.1153	44.25	0.50%
48h	4x4	ZZI-J1	gurobi	6.1283	1.37	0.40%
48h	8x8	ZZI-J1	cplex	6.0687	572.55	0.50%
48h	8x8	ZZI-J1	gurobi	6.0893	19.56	0.37%
48h	4x4	ZZI-K1	cplex	6.1134	280.08	0.50%
48h	4x4	ZZI-K1	gurobi	6.1260	3.81	0.35%
48h	8x8	ZZI-K1	cplex	6.0688	378.48	0.50%
48h	8x8	ZZI-K1	gurobi	6.0928	10.87	0.44%
48h	4x4	C-K1	cplex	6.1134	333.48	0.50%
48h	4x4	C-K1	gurobi	6.1151	2.89	0.19%
48h	8x8	C-K1	cplex	8.2120	3600.00	28.38%
48h	8x8	C-K1	gurobi	6.0952	229.33	0.48%
48h	16x16	ZZI-J1	gurobi	6.0817	30.56	0.36%
48h	16x16	ZZI-K1	gurobi	6.0832	71.00	0.39%
48h	16x16	C-K1	gurobi	-	-	- %
168h_S	8x8	ZZI-J1	gurobi	4.8732	133.61	0.29%
168h_S	16x16	ZZI-J1	gurobi	4.8712	267.63	0.45%
168h_S	8x8	ZZI-K1	gurobi	-	-	- %
168h_S	16x16	ZZI-K1	gurobi	-	-	- %
168h_S	8x8	C-K1	gurobi	4.8806	374.41	0.43%
168h_S	16x16	C-K1	gurobi	-	-	- %
168h_W	8x8	ZZI-J1	gurobi	19.1052	40.83	0.38%
168h_W	16x16	ZZI-J1	gurobi	19.0596	224.11	0.26%
168h_W	8x8	ZZI-K1	gurobi	19.1188	272.77	0.48%
168h_W	16x16	ZZI-K1	gurobi	-	-	- %
168h_W	8x8	C-K1	gurobi	19.1277	3150.87	0.49%
168h_W	16x16	C-K1	gurobi	-	-	- %

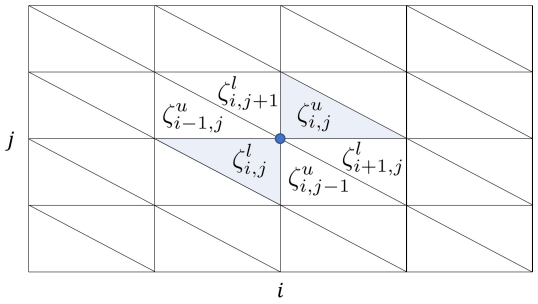

Fig. 10. Classic formulation with a binary variable per triangle

constraint (31a) forces that only one triangle of the mesh must be active. In addition, (31b) ensures that in order for θ_{ij} to be different from zero, at least one of the surrounding triangles must be active.

$$\sum_{i\in I}\sum_{j\in J}\zeta^u_{i,j}+\zeta^l_{i,j}=1 \tag{31a}$$

$$\begin{aligned}\theta_{ij} \le\ & \zeta^u_{i,j}+\zeta^l_{i,j+1}+\zeta^u_{i-1,j}\\ & +\zeta^l_{i,j}+\zeta^u_{i,j-1}+\zeta^l_{i+1,j} \quad \forall i\in I, \forall j\in J\end{aligned} \tag{31b}$$

where it is assumed that the binary variables with subscripts $i-1$, $j-1$, $(i+1,\ j+1)$ are null for the first (last) elements of I and J. In addition, $\zeta^l_{1,j}=\zeta^u_{n+1,j}=0, \forall j\in J$, and $\zeta^l_{i,1}=\zeta^u_{i,m+1}=0, \forall i\in I$.

VI. CONCLUSIONS

This paper addresses the modeling of non-linear losses in Li-Ion batteries. It proposes alternative expressions to those used in state-of-the-art, which model losses based on the battery's state of charge and the power charged or discharged in each period. Regarding the computational performance, the presented zig-zag approaches outperform the classical method, especially in instances with detailed grids for large problems. In particular, the ZZI-J1 exhibits superior behavior in the analyzed cases.

ACKNOWLEDGEMENTS

The first author would like to thank Prof. Andy Sun for the support received to undertake a research stay at Massachusetts Institute of Technology (MIT) where part of this research was carried out, and to Pontifical Comillas University for the received mobility grant.

REFERENCES

[1] J. Huchette and J. P. Vielma, "Nonconvex piecewise linear functions: Advanced formulations and simple modeling tools," *Operations Research*, May 2022. [Online]. Available: https://doi.org/10.1287/opre.2019.1973

[2] M. F. Zia, E. Elbouchikhi, and M. Benbouzid, "Microgrids energy management systems: A critical review on methods, solutions, and prospects," *Applied Energy*, vol. 222, pp. 1033–1055, Jul. 2018.

[3] A. Fotouhi, D. J. Auger, K. Propp, S. Longo, and M. Wild, "A review on electric vehicle battery modelling: From lithium-ion toward lithium–sulphur," *Renewable and Sustainable Energy Reviews*, vol. 56, pp. 1008–1021, Apr. 2016. [Online]. Available: https://doi.org/10.1016/j.rser.2015.12.009

[4] C. M. Shepherd, "Design of Primary and Secondary Cells: II . An Equation Describing Battery Discharge," *Journal of The Electrochemical Society*, vol. 112, no. 7, 1965.

[5] O. Tremblay and L.-A. Dessaint, "Experimental Validation of a Battery Dynamic Model for EV Applications," *World Electric Vehicle Journal*, vol. 3, no. 2, pp. 289–298, Jun. 2009. [Online]. Available: https://www.mdpi.com/2032-6653/3/2/289

[6] T. M. Inc., "Matlab version: 9.14.0.2239454 (r2023a) update 1," Natick, Massachusetts, United States, 2023. [Online]. Available: https://www.mathworks.com

[7] T. A. Nguyen and M. L. Crow, "Stochastic Optimization of Renewable-Based Microgrid Operation Incorporating Battery Operating Cost," *IEEE Transactions on Power Systems*, vol. 31, no. 3, pp. 2289–2296, May 2016.

[8] H. Shuai, J. Fang, X. Ai, J. Wen, and H. He, "Optimal Real-Time Operation Strategy for Microgrid: An ADP-Based Stochastic Nonlinear Optimization Approach," *IEEE Transactions on Sustainable Energy*, vol. 10, no. 2, pp. 931–942, Apr. 2019.

[9] D. A. Babayev, "Piece-wise linear approximation of functions of two variables," *Journal of Heuristics*, vol. 2, no. 4, pp. 313–320, 1997. [Online]. Available: https://doi.org/10.1007/bf00132502

[10] C. D'Ambrosio, A. Lodi, and S. Martello, "Piecewise linear approximation of functions of two variables in milp models," *Operations Research Letters*, vol. 38, no. 1, p. 39–46, Jan. 2010. [Online]. Available: http://dx.doi.org/10.1016/j.orl.2009.09.005

[11] J. P. Vielma and G. L. Nemhauser, "Modeling disjunctive constraints with a logarithmic number of binary variables and constraints," *Mathematical Programming*, vol. 128, no. 1-2, pp. 49–72, Jul. 2009. [Online]. Available: https://doi.org/10.1007/s10107-009-0295-4

[12] S. Wang, J. Liu, H. Chen, R. Bo, and Y. Chen, "Modeling state transition and head-dependent efficiency curve for pumped storage hydro in look-ahead dispatch," *IEEE Transactions on Power Systems*, vol. 36, no. 6, pp. 5396–5407, Nov. 2021. [Online]. Available: https://doi.org/10.1109/tpwrs.2021.3084909

[13] D. Domínguez-Barbero, J. García-González, and M. A. Sanz-Bobi, "Twin-delayed deep deterministic policy gradient algorithm for the energy management of microgrids," *Engineering Applications of Artificial Intelligence*, vol. 125, p. 106693, 2023. [Online]. Available: https://www.sciencedirect.com/science/article/pii/S0952197623008771